Lawrence Berkeley National Laboratory

Title

FPGA-Based Optical Cavity Phase Stabilization for Coherent Pulse Stacking

Permalink

https://escholarship.org/uc/item/92h0x1fh

Journal

IEEE Journal of Quantum Electronics, 54(1)

ISSN

0018-9197

Authors

Xu, Yilun
Wilcox, Russell
Byrd, John
et al.

Publication Date

2018

DOI

10.1109/jqe.2017.2775698

Copyright Information

Peer reviewed

FPGA-Based Optical Cavity Phase Stabilization for Coherent Pulse Stacking

Yilun Xu, Russell Wilcox, John Byrd, Lawrence Doolittle, Qiang Du, Gang Huang [ID], Yawei Yang, Tong Zhou, Wim Leemans, *Fellow, IEEE*, Almantas Galvanauskas, John Ruppe, Chuanxiang Tang, and Wenhui Huang

Abstract— Coherent pulse stacking (CPS) is a new time-domain coherent addition technique that stacks several optical pulses into a single output pulse, enabling high pulse energy from fiber lasers. We develop a robust, scalable, and distributed digital control system with firmware and software integration for algorithms, to support the CPS application. We model CPS as a digital filter in the Z domain and implement a pulse-pattern-based cavity phase detection algorithm on an field-programmable gate array (FPGA). A two-stage (2+1 cavities) 15-pulse stacking system achieves an 11.0 peak-power enhancement factor. Each optical cavity is fed back at 1.5 kHz, and stabilized at an individually-prescribed round-trip phase with 0.7 deg and 2.1 deg rms phase errors for Stages 1 and 2, respectively. Optical cavity phase control with nanometer accuracy ensures 1.2% intensity stability of the stacked pulse over 12 h. The FPGA-based feedback control system can be scaled to large numbers of optical cavities.

Index Terms— Fiber lasers, optical pulses, optical resonators, optical variables control.

I. Introduction

DEVELOPMENT of advanced kW-class ultrafast lasers will have a significant impact on laser-driven particle accelerator systems [1]. However, inefficiency of thermal handling capability currently limits the repetition rate of high energy systems [2]. A different laser technology is needed for high repetition rate. Fibers are superior in many ways, *i.e.,* demonstrated high average power, good heat removal

Y. Xu is with the Accelerator Technology and Applied Physics Division, Lawrence Berkeley National Laboratory, Berkeley, CA 94720 USA, and also with the Department of Engineering Physics, Tsinghua University, Beijing 100084, China (e-mail: yilunxu@lbl.gov; xu-yl13@mails.tsinghua.edu.cn).

R. Wilcox, J. Byrd, L. Doolittle, Q. Du, G. Huang, Y. Yang, T. Zhou, and W. Leemans are with the Accelerator Technology and Applied Physics Division, Lawrence Berkeley National Laboratory, Berkeley, CA 94720 USA (e-mail: rbwilcox@lbl.gov; jmbyrd@lbl.gov; lrdoolittle@lbl.gov; qdu@lbl.gov; ghuang@lbl.gov; yaweiyang@lbl.gov; tongzhou@lbl.gov; wpleemans@lbl.gov).

A. Galvanauskas and J. Ruppe are with the Center for Ultrafast Optical Science, University of Michigan, Ann Arbor, MI 48109 USA (e-mail: almantas@umich.edu; jmruppe@umich.edu).

C. Tang and W. Huang are with the Department of Engineering Physics, Tsinghua University, Beijing 100084, China (e-mail: tang.xuh@tsinghua.edu.cn; huangwh@mail.tsinghua.edu.cn).

Color versions of one or more of the figures in this paper are available online at http://ieeexplore.ieee.org.

Digital Object Identifier 10.1109/JQE.2017.2775698

efficiency, excellent beam quality, and stable alignment [3], but challenges such as small aperture and narrow bandwidth limit output energy and pulse width. Fortunately, we can increase energy and bandwidth by adding pulses temporally [4], [5], spatially [6], [7] and spectrally [8].

The temporal addition is achieved either with resonant cavities [4] or with optical delay lines [5]. Passive resonant cavities without any intra-cavity components eliminate the complexity of incorporating mechanical rotating-mirrors, while polarizing beam splitters (PBS) are introduced into optical delay lines for the combination efficiency. The use of resonant cavities leads to small-footprint arrangements, compared to optical delay lines whose lengths increase exponentially with the number of pulse division stages. The phase stabilization with optical delay lines is based on a single detector at the system output, allowing for the dithering technique such as the locking of optical coherence via single-detector electronic-frequency tagging (LOCSET) [9]. However, the system can switch among several undesirable stable states due to momentary phase perturbations, which is found to be intrinsic to the temporal addition using optical delay lines in combination with the LOCSET phase stabilization [10]. Instead of the frequency-tagged dithering method, the technique reported here for resonant cavities is a direct and deterministic phase stabilization method, which means that the individual round-trip phase for each cavity can be computed accurately and each cavity can be locked to any specified phase. Based on the stabilization of the optical cavity phase, coherent stacking of several short pulses into a single output pulse in the fiber amplifier system is a promising technique for extracting all available energy from a fiber amplifier, combining high average power and high repetition rate. Stacking of 81 pulses in a 10 mJ pulse train has been demonstrated, enabling high energy pulse outputs with low nonlinear effects [11].

Timing and synchronization are essential for ultrafast pulse addition, and scalable controls are needed for a complex optical system. Here we develop a robust, scalable and distributed digital control system, which combines high precision digital RF feedback control and stable optical cavities to support the coherent pulse stacking application. Leveraging of capabilities of state-of-the-art high-speed digitizer, field-programmable gate array (FPGA) and deterministic high-throughput data exchange network, this control system is a potential open source toolbox in general coherent combination control.
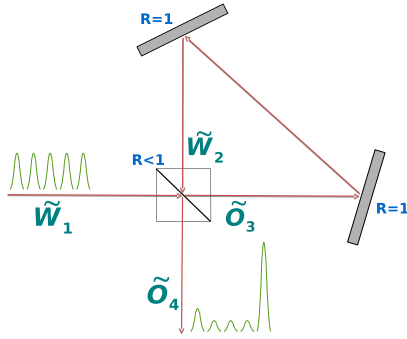
Fig. 1. Physical model of pulse interference.

II. THEORY OF COHERENT PULSE STACKING AND CAVITY PHASE STABILIZATION

A. Z Domain Modeling of Coherent Pulse Stacking

In the coherent pulse stacking scheme, pulses are added in a Gires-Tournois interferometer, which is composed of a partially reflecting front mirror and several completely reflecting beam-folding mirrors [12]. As shown in Fig. 1, the initial pulses of the tailored optical pulse burst enter the reflecting resonant cavity and interfere destructively at the cavity output port, thus storing optical energy inside the resonant cavity. Later, the final pulse in the burst produces a constructive interference with the previous intra-cavity pulses at the output port, so that all stored energy is extracted from the resonant cavity into a single output pulse.

If the round-trip length is L, the intra-cavity round-trip optical phase shift is

$$\varphi = \frac{2\pi L}{\lambda_0}, \tag{1}$$

where λ_0 is the optical wavelength. The condition of interference is that the incident pulse and the circulating intra-cavity pulse arrive at the front-mirror simultaneously, that is to say, the round-trip phase φ is corresponding to the pulse interval ΔT. To describe the first-order physics of a front-mirror as a beam combiner/splitter, we will employ the Z-transform, which is borrowed from microwave electronics and filter design. In signal processing terms, we are seeking a solution to the zero-state response in a discrete-time linear time invariant (DLTI) system.

The input and output pulse electric fields at both sides of the front-mirror can be described by a scattering matrix

$$\begin{bmatrix} \widetilde{O}_4 \\ \widetilde{O}_3 \end{bmatrix} = \begin{bmatrix} r & jt \\ jt & r \end{bmatrix} \begin{bmatrix} \widetilde{W}_1 \\ \widetilde{W}_2 \end{bmatrix}, \tag{2}$$

where input waves ($\widetilde{W}_1$, $\widetilde{W}_2$) and output waves ($\widetilde{O}_3$, $\widetilde{O}_4$) are all complex numbers. Here r and t are the reflection coefficient and the transmission coefficient respectively, which are related by $r^2 + t^2 = 1$ for a lossless mirror. We use the Z-transform formalism to express the delay line in the context of a pulsed laser,

$$\widetilde{W}_2 = z^{-1}\alpha e^{j\varphi}\widetilde{O}_3, \tag{3}$$

where α is the transmission loss coefficient. Here we call the round-trip phase φ the "cavity phase".

The input-output transfer function will be

$$H(z) = \frac{Y(z)}{X(z)} = \frac{r - \alpha e^{j\varphi}z^{-1}}{1 - r\alpha e^{j\varphi}z^{-1}}, \tag{4}$$

where the transfer function $H(z)$ is the linear mapping of the Z-transform of the input $X(z)$ to the Z-transform of the output $Y(z)$. Since the system is passive, it is important that the pole is always inside the unit circle, representing stability. Compared with a time-domain analysis [13], it is much easier to express the system transfer function of cascaded cavities as

$$H_{\text{cascaded}}(z) = \prod_i H_i(z). \tag{5}$$

The coherent pulse stacker acts as a digital filter which is characterized by cavity phase and front-mirror reflectivity. Provided the cavity is lossless and there is no additional loss due to imperfect interference, transmission loss coefficient α is 1 and front-mirror reflectivity r is constant. The cavity phase φ will determine the interference, and the efficiency of the system is related to the ability to control the phase accumulated by optical pulses in each path so as to ensure a constructive interference.

B. Simulation for Two-Stage Stacking

Properly configured sequences of multiple optical cavities will achieve a peak-power enhancement factor η, defined as the ratio between peak powers of the stacked output and highest amplitude incident pulse. Cascading equal round-trip cavities forms a "stacking stage", where the enhancement factor grows linearly with the number of cavities. For example, in a stacking stage, one cavity with 3 pulses obtains the enhancement factor of 2.6, two cavities with 5 pulses achieve the enhancement factor of 4.6, and so on.

The output stacked pulse sequence of the previous stage can be used as the input pulse train of the next stage. The cavity round-trip length in the later stage is longer than that in the preceding stage because of the larger pulse period delay. Cascading M stages obtains the peak-power enhancement

$$\eta_{\text{total}} = \prod_{m=1}^{M} \eta_m. \tag{6}$$

With the implementation of the Z-transform model, coherent pulse stacking is simulated in a two-stage configuration (two short cavities in Stage 1 and one long cavity in Stage 2). As shown in Fig. 2, 15 equal-amplitude pulses (5×3) are stacked into one single output pulse in multiplexed 2+1 cavities. Three sets of 5 pulses in Stage 1 make up an equal-amplitude 3-pulse train, then three stacked pulses from Stage 1 will be stacked into a single output pulse in the longer cavity in Stage 2. This two-stage stacking obtains a theoretical peak-power enhancement factor of 12.0 (4.6×2.6) according to (6).

The satellite-pulse contrast ratio γ, defined as the ratio between peak powers of the output stacked pulse and its previous pulse, is 25 dB in theory for the above configuration. In order to characterize the pulse energy loss in a resonant cavity, stacking efficiency χ is defined as the ratio between the energy of the single stacked pulse and the total energy of
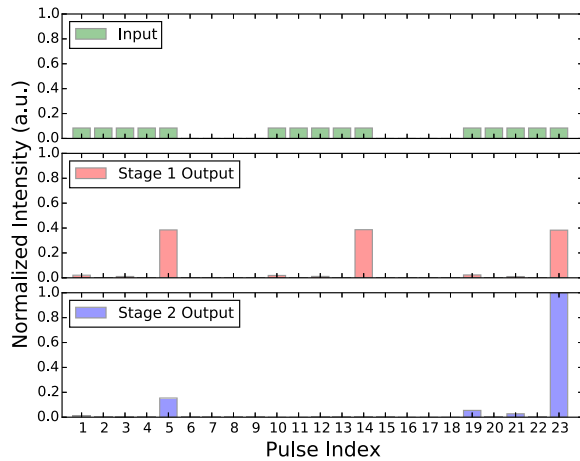
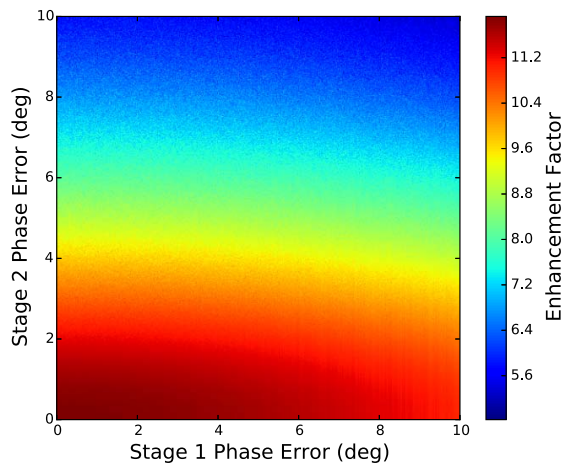Fig. 2. Simulation for 15-pulse stacking in 2+1 cavities.

Fig. 3. Peak-power enhancement factor vs RMS cavity phase error.

Fig. 4. Stack pulses, phase probe pulses and bias probe pulses form a pulse sequence.

the incident pulse burst. While the later pulses in a burst are the ones being stacked, the very first pulse is to establish the optical cavity field beforehand. The first input pulse injects the initial energy into the cavity and provides the initial intra-cavity pulse for the following interference, so the very first output pulse causes a pre-pulse which cannot be eliminated. The stacking efficiency is 80% here, while the pre-pulse accounts for 12% of the total energy. The pre-pulse can be made relatively small and far away from the stacked pulse by increasing the length of the incident pulse burst. The simulation reported here is for a specific set of 2+1 cavities with 15 equal-amplitude input pulses, but is universally applicable to any number of cavities and all possible configurations.

C. Stabilization of Optical Cavity Phase

Feedback control of cavity phase is one of the key technologies to realize coherent pulse stacking, and is critical to the system performance and robustness. The cavity phase is stabilized within a fraction of optical wavelength against thermal drift, acoustic perturbation and mechanical vibration by proper feedback control of a piezo-driven mirror for each cavity. Failure to maintain the cavity phase matching translates into a decrease of the stacking efficiency and combined peak power, as shown in Fig. 3. For instance, stabilizing the cavity phase in Stage 1 and Stage 2 with errors less than 1.0 deg and
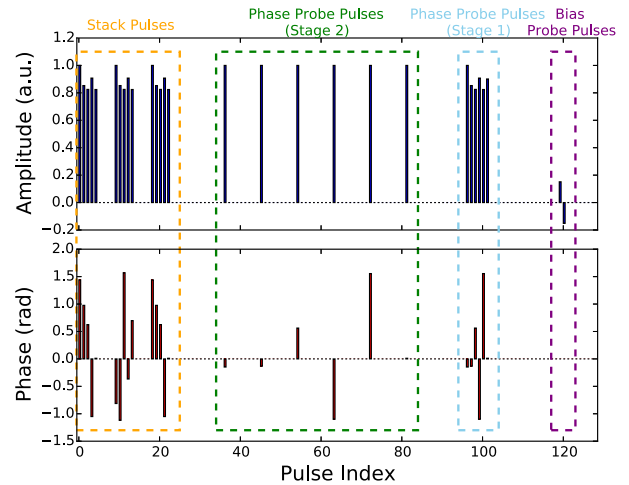
2.5 deg respectively will keep the peak-power enhancement higher than 91% of its theoretical maximum.

Our scheme for stabilizing the cavity phase is based on measuring the intensities of each pulse from each cavity. The extraction of cavity phase from a limited measurement, where a photodiode can only detect pulse intensity, can be treated as a "grey box model", which combines a partial theoretical structure with data to complete the model. Since each pulse in a burst is affected by a different number of round-trips, there will be differing intensity functions as the cavity phase is tuned over 2π. Therefore, it is possible to identify the cavity phase by a unique combination of pulse intensities. A pulse-pattern-based cavity phase detection algorithm is employed in our feedback control system. Instead of using the stack pulse train itself, a special phase probe pulse burst is injected together with the stack pulse train to diagnose the optical cavity fluctuation and lock the cavity phase according to the described cavity control model. The stack pulse train (15 pulses), the phase probe pulse train (6 pulses for Stage 1 and 6 pulses for Stage 2) and the bias probe pulse train (2 pulses, to monitor the amplitude modulator bias point) form a pulse sequence, as shown in Fig. 4. The pulse interval is 2.5 ns, so the delay of each pulse is this interval times the position within the burst, or "pulse index".

Fig. 5 illustrates the digital processing chain of cavity phase extraction and laser feedback. The ADC (analog-to-digital converters) samples the pulse signal from a photodiode. A DPRAM (dual port ram) records the pulse intensity data, while a circular buffer stores data streams simultaneously. Six specified channels, which are corresponding to 6 phase probe pulses, are selected for cavity phase diagnosis. In our current experiment, low optical power levels require amplified high-speed photodiodes. These produce electronic noise, so noise reduction needs to be employed. Leveraging of the fast processing and real-time performance provided by the FPGA, a cascaded integrator-comb (CIC) filter is included in the control feedback loop as moving-average digital processing for noise suppression. The CIC filter, which utilizes only addition and subtraction, and requires no multiplication operations, is an efficient and economical implementation in FPGA,
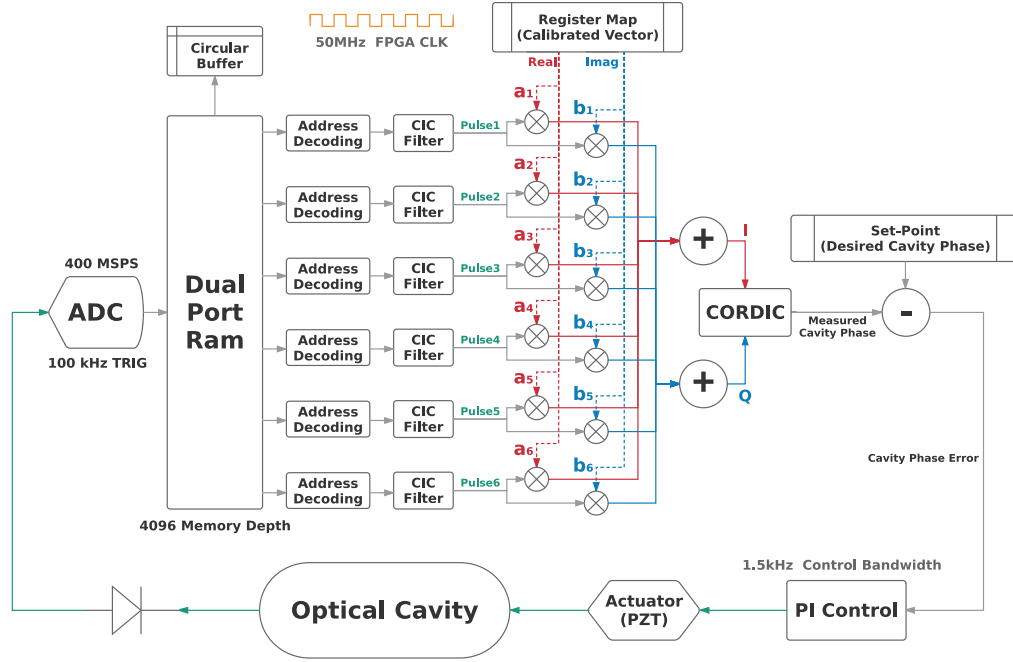
Fig. 5. Data flow of cavity control module.

with characteristics of low pass frequency and linear phase response.

Intensities (averaged by CIC filters) of N phase probe pulses (N is 6 here) at the cavity output port can be represented as a vector: $\vec{o}(\varphi) = [O_1, O_1, \cdots, O_N]$. The cavity phase can be computed simply and quickly by a dot-product of the N-long optical vector measurement with a known complex vector, which we call a "template vector", according to

$$\vec{o}(\varphi)\cdot\vec{v} = e^{j\varphi}, \tag{7}$$

where $\vec{v}$ is the template vector which requires an initial calibration beforehand, and φ is the cavity phase. The FPGA does the dot product operation in real part and imaginary part to acquire the in-phase component (I) and the quadrature component (Q) respectively, followed by a CORDIC (COordinate Rotation DIgital Computer) module extracting the cavity phase information. The CORDIC algorithm is implemented as a rectangular-to-polar conversion due to the efficiency of calculating inverse trigonometric functions in FPGAs. Once optical matrix calculations are finished and cavity phase is obtained, a PI loop is implemented to drive the piezo to lock the optical cavity at an intended phase.

To calibrate the template vector, one can vary the cavity phase over 2π while observing the output from a phase probe pulse train. Rewriting (7) in matrix form yields the complex template vector in the calibration procedure:

$$
\begin{bmatrix} a_1 + b_1 j \\ a_2 + b_2 j \\ \vdots \\ a_N + b_N j \end{bmatrix} = \begin{bmatrix} O_{1,1} & O_{1,2} & \ldots & O_{1,N} \\ O_{2,1} & O_{2,2} & \ldots & O_{2,N} \\ \vdots & \vdots & \ddots & \vdots \\ O_{M,1} & O_{M,2} & \ldots & O_{M,N} \end{bmatrix} \Big\backslash \begin{bmatrix} e^{j2\pi\frac{1}{M}} \\ e^{j2\pi\frac{2}{M}} \\ \vdots \\ e^{j2\pi\frac{M}{M}} \end{bmatrix}, \tag{8}
$$

where M is the scanning resolution in one whole cycle of the cavity phase, and a and b are real and imaginary parts respectively of the template vector. The complex template vector is the least-squares solution to the above linear matrix equation.

III. Stacking Stabilization Experiment

A. Optical System Architecture

The experimental system is shown in Fig. 6. The mode-locked laser oscillator provides an optical pulse train at 400 MHz, which is coupled into a polarization-maintaining single-mode fiber. An amplitude modulator gates out the pulse train, followed by a phase modulator imprinting the required phase. The tailored pulse train is then launched into Stage 1 consisting of two short cavities. The pulse train out of Stage 1 enters the long cavity for the second-stage stacking, finally combining all pulses into one.

In the optical system, an intrinsically stable Herriott cell with re-entrant design is used as the short cavity for Stage 1 [14], [15]. A partially reflecting beam-splitter cube (power reflectivity is 0.5) is introduced into one beam in the Herriott cell, adding only one extra optic, and using standard high-reflecting curved mirrors. The configuration of the long cavity for Stage 2 is also a Herriott cell, folded in half at the central plane by a flat mirror. This mirror has a partially reflecting area (power reflectivity is 0.4) and a high-reflecting area, eliminating any intra-cavity optics [16]. Here the long cavity in Stage 2 is 9 times longer than the short cavity in Stage 1.

B. Control System Architecture

In the control system, the controller processes pulse intensities detected by multiple photodiodes to compensate for thermal, acoustic and mechanical perturbations inside optical
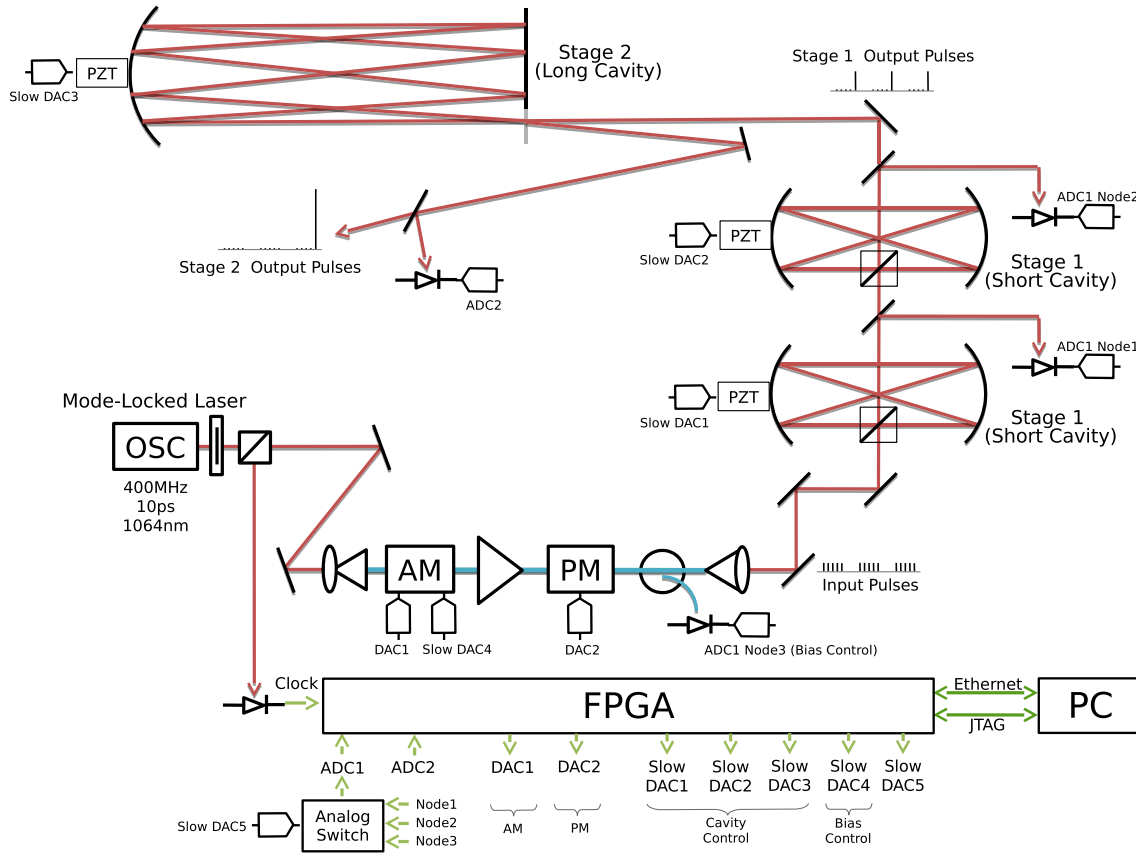
Fig. 6.   Experimental setup for coherent pulse stacking.

cavities in real time. Piezo-driven mirrors, amplitude/phase modulators, and analog switches are addressed by the distributed control network to stabilize each local process using corresponding diagnostics, so that the pulse stacking could be broken down into individual controllable local loops.

The Xilinx ML605 is the FPGA carrier in our hardware architecture, with an FMC (FPGA mezzanine card) daughter card (FMC110 from 4DSP) providing high-speed ADCs and DACs (digital-to-analog converters), and an expansion card (Pmod DA4 from Digilent) providing slow DACs. In the experimental control system, the mode-locked laser oscillator generates a 1064 nm optical beam at 400 MHz with 10 ps pulse width. ADCs and DACs are clocked by the in-burst repetition rate of 400 MHz, while the FPGA is clocked by 1/8 of 400 MHz with the data stream aspect ratio of 1:8. The FPGA drives two synchronous DACs to modulate the pulse amplitude and phase in the fiber-coupled electro-optic modulators. Dual-channel synchronous ADCs acquire pulse intensities from multiple photodiodes to pick up the optical cavity information. The two DACs and two ADCs, which are built in the FMC110 card, are all triggered by 100 kHz inter-burst repetition rate which is divided by 4096 from the 400 MHz clock. Piezo mounted mirrors in each cavity are driven by the FPGA through slow DACs on the Pmod DA4 card for cavity length stabilization. The Pmod DA4 card also provides some more slow DACs for modulator bias control and analog switch control (which switches the different photodiode channels leading to one ADC).

C. Amplitude and Phase Modulation

It is necessary to modulate the laser pulse train in amplitude and phase, so that pulses with any amplitude or phase can be output to the optical cavities. Since DAC output voltages will need to produce 0-100% modulation of amplitude, and $\pm\pi$ modulation of phase, we need to know voltage-to-amplitude and voltage-to-phase factors that will be used to specify the DAC data. Our amplitude modulation (AM) and phase modulation (PM) systems have been calibrated to provide these factors.

The amplitude modulator is nonlinear with a $\sin^2$ function. It is important to know the "V_π" of the modulator, which is the voltage which causes a change between 100% and zero transmission, or equivalently the voltage which creates a relative phase shift from zero to π between the two arms of the Mach-Zehnder interferometer. One can know the relative phase from the voltage, and further know the transmission via the $\sin^2$ function from the relative phase. Amplitude modulator calibration consists of applying a ramp of voltage and observing the output pulse amplitude. The fast DAC produces a slowly varying series of voltage steps, over a range larger than the specified V_π for the modulator, while the fast ADC samples the resulting signal accordingly.
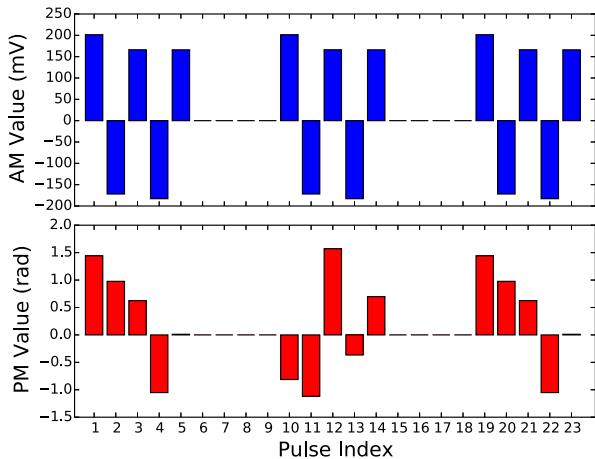
Fig. 7. Amplitude modulation (AM) and phase modulation (PM) data for DACs in the 2+1 configuration.

The phase modulator provides a linear phase shift with voltage, so only the V_π needs to be measured during phase calibration. One can multiply V_π by the desired phase to get the voltage data. For the acquisition of V_π, we generate a test pulse train, which consists of three equal-amplitude pulses, with "zero" phase applied to the first pulse and "$\pm\Delta V$" phases applied to the other two. We then program the slow DAC to scan the cavity phase over 2π and observe the amplitude of one of the output pulses. The cavity here acts as a diagnostic interferometer. The 3-pulse test train goes into the cavity, and an output pulse train is observed by the ADC. The first output pulse is the first one reflected from the cavity input mirror. We are interested in the 4th pulse out of the cavity, whose amplitude has two humps during a scan of the cavity phase of 2π. Two humps are equal only in the condition of "pulse phase is π", that is "$\Delta V = V_\pi$". Thus, if we scan the cavity phase (using slow DAC) and vary ΔV (using fast DAC) until the humps are equal, we have found the V_π for the phase modulator.

In the modulation system, a pulse burst is carved out of the laser source by an amplitude modulator, then phase is controlled through a phase modulator. We have to derive modulation functions for both these modulators. For large numbers of pulses, it is efficient to apply the equal-amplitude modulation to the input pulse train. To derive the phase modulation function, we know that the first pulses of the optical pulse burst interfere destructively while the final pulse interferes constructively. Working backward from the desired output, we set the output single stacked-pulse to 1 and preceding satellite-pulses to 0. It is then easy to reverse the numerator and denominator of the system transfer function in order to calculate input pulses, which can be related to $X(z)$ as

$$X(z) = H^{-1}(z) \cdot Y(z) = \frac{1 - r\alpha e^{j\varphi} z^{-1}}{r - \alpha e^{j\varphi} z^{-1}} \cdot Y(z). \qquad (9)$$

From this equation, we derive the driving functions for the amplitude and phase modulators, as shown in Fig. 7. The AC-coupled DAC, which drives the amplitude modulator, will distort an equal-amplitude waveform. To alleviate this high-pass filtering, the modulation values for AM are

alternated in polarity, and made slightly unequal in order to compensate for filtering during the burst, to guarantee an equal-amplitude optical pulse train output from the modulator.

D. Bias Control

For pulse applications, it is necessary to control the amplitude modulator bias voltage in order to fix the working point at the minimum of its transfer function. Digital control of the amplitude modulator bias has been implemented in the feedback loop, so that we can stabilize the operating point of the modulator by varying the bias voltage applied to the DC electrode of the device.

Three voltages (plus, zero and minus) are added to the modulation signal through a fast DAC while the ADC acquires readings corresponding to those voltage steps. The location of the operating point on the transfer function curve is determined by the ADC reading. We vary the bias voltage to keep the optical output minimum, where the plus voltage results in a reading that is equal to the minus voltage reading, while the zero voltage reading is the lowest of these three readings. Only integral control needs to be implemented in the feedback loop to eliminate the residual steady-state error.

Extinction ratio characterizes the ON state versus OFF state modulator transmission. In our system, extinction ratio of the modulator is 28 dB which suits the stacking extinction requirement.

IV. EXPERIMENTAL RESULTS

A. Cavity Perturbation Measurements

Optical cavity perturbations, including long-term drift and short-term noise, determine the stacking efficiency and the optical pulse stability. Compensating for the cavity perturbations in real time requires feedback control.

The long-term slow drift of the optical cavity can be characterized by the coefficient of thermal expansion (CTE). For the short cavity with round-trip length of 0.75 m, 1°C temperature change over night at $\sim 10^{-5}$ m $\cdot$ °C/m CTE level results in $\sim 7.5\,\mu$m cavity length drift ($\sim 1.9\,\mu$m piezo displacement), which is corresponding to ~ 44 radians cavity phase drift (about 7 cycles) for the 1064 nm optical beam. Note that the slow drift is linear with the cavity round-trip length, and the long cavity is 9 times longer than the short cavity in our optical system, so it causes $\sim 67.5\,\mu$m cavity length drift ($\sim 8.4\,\mu$m piezo displacement) in the long cavity. The tens of microns slow drift will be compensated by the feedback control loop, although we reset the control voltage after each wave of compensation. Since we are working with 10 ps pulses in this control development system, the group delay can be allowed to vary. In an actual ultrafast system, an additional long range cavity length control would be used.

Short-term noise measurements have been made to facilitate the control system design. Since the cavity phase is controlled to ensure the stability of the stacked pulse, we measure the noise spectrum of the cavity phase and the stacked pulse. Fig. 8 shows the pulse trains obtained when the system is stabilized. The enhancement factor and the stacking efficiency are 11.0 and 76%, compared to the theoretical limits
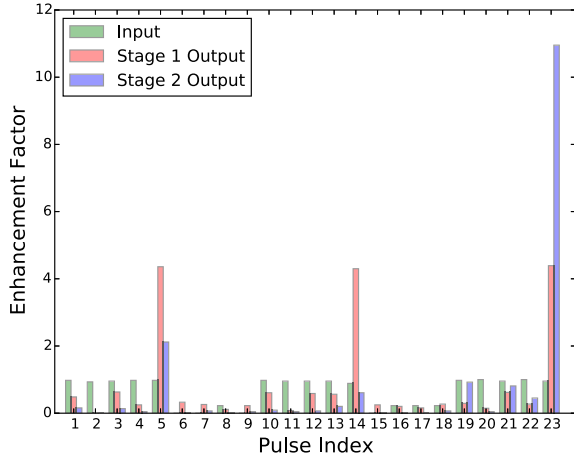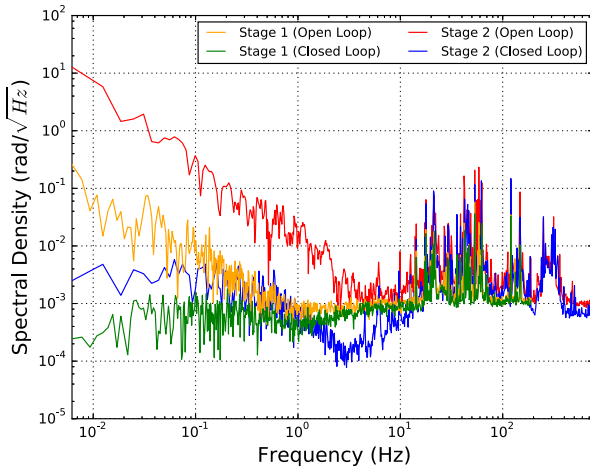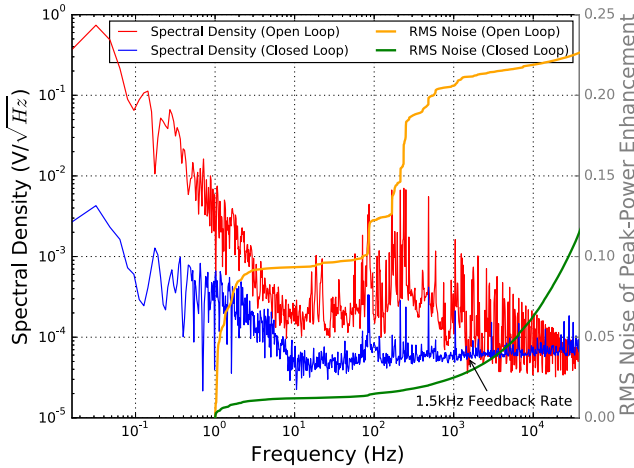
Fig. 8. Experimental result for 15-pulse stacking in 2+1 cavities.

(a)

(b)

Fig. 9. Short-term noise measurements. (a) Noise spectrum of the cavity phase. (b) Noise spectrum of the stacked pulse.

of 12.0 and 80% respectively. Fig. 9(a) shows the noise spectrum of the cavity phase sampled at 1.5 kHz rate (implementing 64 times averaging with CIC filter) over 3 minutes. Because Cavity 1, Cavity 2, bias control and a monitor channel

share the same ADC via an analog switch, the feedback control rate of Stage 1 is 1/4 of Stage 2 (1.5 kHz/4=375 Hz). We estimate the noise spectrum by applying discrete Fourier transform (DFT) with Hanning window function due to its low aliasing. The DC average is not usually of interest as a result of the DFT processing, hence we normally remove it from the time series before the FFT (fast Fourier transform) is performed. Comparing the noise spectrum of Stage 1 and Stage 2, the optical cavity will be noisier as the cavity length gets longer.

In our system, the control bandwidth is limited by a piezo-driven mirror whose resonant frequency is 1.6 kHz. So we implement the feedback control at a rate of 1.5 kHz. In the stacked pulse noise measurement, a photodiode detects the output stacked pulse, and the FPGA records the pulse data in a circular buffer without losing any timing information. Fig. 9(b) shows the noise spectrum of the single stacked pulse sampled at 100 kHz rate (stacked pulse powers are recorded as raw data without averaging) over 1 minute. The amplitude spectral density has units of $V/\sqrt{Hz}$. The system noise arises from $1/f$ noise, broadband optical and electronic noise, thermal pickup and acoustic pickup. For frequencies in the feedback bandwidth, the noise is specified with loop closed and running at maximum gain. The closed loop suppresses the in-band noise significantly compared to the open loop. Broadband (white) noise is minimized by proper selection of low noise components. The integral RMS noise in the frequency domain is equal to the standard deviation in the time domain. To convert the amplitude spectral density in the frequency domain to the RMS fluctuation in the time domain, one can square the amplitude spectral density to get the power spectral density (PSD), then integrate the PSD across the desired bandwidth, and take the square root of the result. As shown in Fig. 9(b), 0.12 integral RMS noise (from 1 Hz to 50 kHz) is the standard deviation of the enhancement factor. The intensity stability, defined as the ratio of standard deviation to mean of the stacked pulse, is 0.12/11.0=1.1% for short term. The crossover point between the open loop and the closed loop spectral density curves in the noise spectrum is the unity gain frequency, which is 1.5 kHz in our system.

B. Long-Term Stabilization Results for Two-Stage Stacking

The stacking system was controlled by the FPGA for 12 hours, while logging the cavity phase error in degrees, the piezo displacement in microns and the stacked pulse intensity.

The phases of Cavity 1 and Cavity 2 in Stage 1 were maintained within 0.4 deg (RMS) and 0.7 deg (RMS), while the phase of Cavity 3 in Stage 2 was stabilized at 2.1 deg (RMS) phase error over 12 hours, as shown in Fig. 10(a). The piezo driven by FPGA compensates for thermal and acoustic perturbations in each cavity for stacking stabilization. The cavity piezo displacement should be the cavity round-trip length change divided by the number of folded paths (4 for Stage 1 and 8 for Stage 2). Fig. 10(b) shows the piezo varies several microns over night, indicating an environmental temperature drop during the night. A small fraction of stacking output is coupled into a photodiode in order to
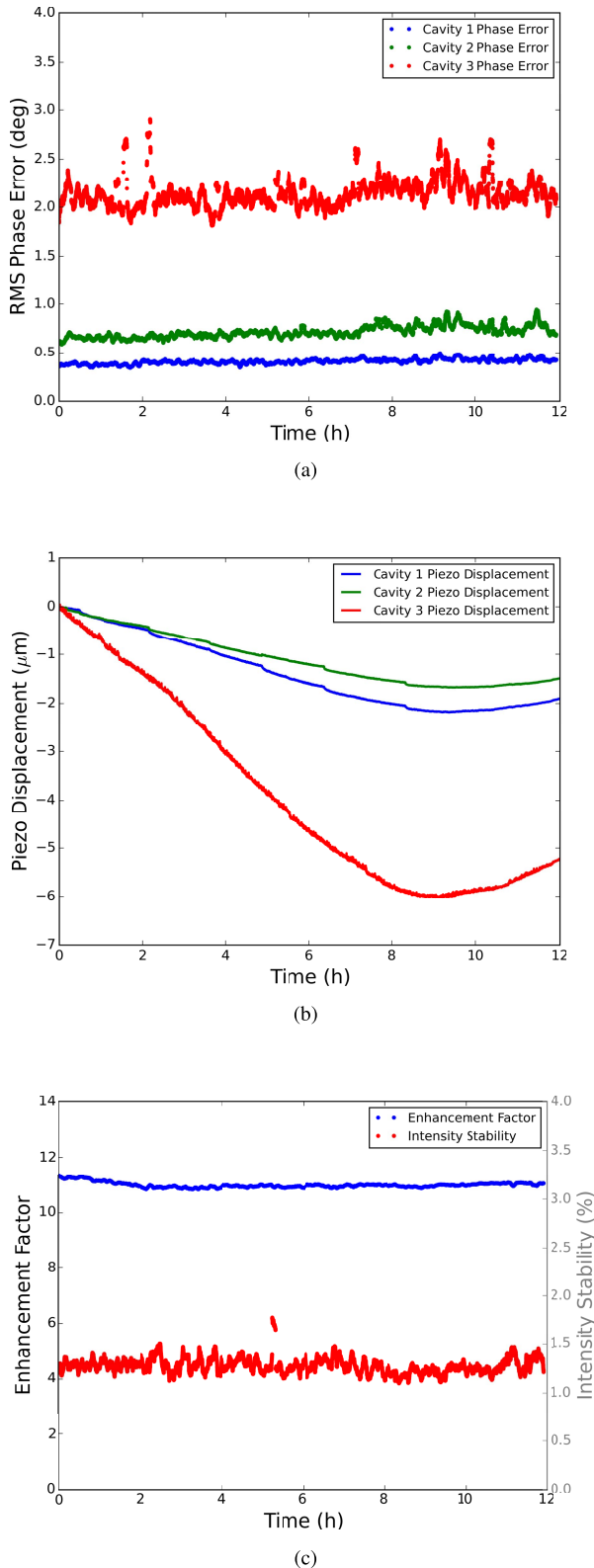
Fig. 10. Long-term stabilization measurements. (a) Cavity phase errors over 12 hours. (b) Cavity piezo displacements over 12 hours. (c) Enhancement factor and stacked pulse intensity stability over 12 hours.

monitor the stacked pulse. Fig. 10(c) shows the peak-power enhancement factor versus time, during which the long-term intensity stability of the single output pulse is kept within 1.2% (RMS). Optical cavity tuning is optimized to increase the peak-power enhancement factor to 11.0 as well as the satellite-pulse contrast ratio to 14 dB, which suit the two-stage stacking requirement.

V. SCALABILITY OF FPGA-BASED COHERENT PULSE STACKING

A. Scaling of Cavity Phase Error

Fluctuations of the cavity round-trip phase are associated with two types of perturbing effects: non-statistical perturbations and statistical perturbations [17]. Non-statistical perturbations can be divided into two categories: the mechanical perturbation which is caused by vibrations that structurally deform the cavity, and the thermal perturbation which is related to the CTE of the cavity materials.

Mechanical vibrations imparted to the optical platform in the frequency region from tens of Hz to hundreds of Hz could excite the resonance modes of the platform or the optical components, as indicated by the sharp peaks shown in Fig. 9(a). With a careful cavity tuning, we conclude that this mechanical perturbation makes the dominant contribution to the cavity phase error. Both the substrate and coating displacements induced by the mechanical perturbation are essentially independent of the cavity length, due to the fact that the fluctuations are localized to the mirror surface [18]. So the cavity phase error caused by the mechanical perturbation will not scale with the multi-stage stacking. To eliminate the mechanical excitation and reduce the mechanical noise, we will float the entire optical platform in the near future. This deployment will significantly isolate the system from the local ambient noise and damp the vibration energy.

The thermal perturbation is the minor phase error source. Taking the differential on both sides of (1) and combining the resulting equation with $\delta L = \alpha_L \cdot \delta T \cdot L$ yield

$$\delta\varphi = \frac{2\pi \cdot \alpha_L \cdot \delta T \cdot L}{\lambda_0}, \tag{10}$$

where α_L is the linear expansion coefficient, δL and δT denote the cavity length variation and the temperature variation. Considering the scalability of CPS, it is not a good thing that the cavity phase variation introduced by the thermal fluctuation grows linearly with the increase of the cavity size. However, since the thermal noise mostly falls into the control bandwidth, the FPGA-based feedback system could significantly compensate for the thermal perturbation and suppress the thermal noise in real time, which has been validated in our experiment. In the near future, we will add a thermal shield and actively control the temperature for the setup to reject the thermal noise even further.

In our system, the statistical perturbation can be treated as the additive white Gaussian noise (AWGN), which does not depend on the cavity length. In general, the standard deviation of the average of samples is reduced from the standard deviation of each individual sample by a factor of the square root of the reciprocal of the number of samples. Thus, by averaging a set of replicate measurements, the signal-to-noise ratio (SNR) will be increased ideally in proportion to the square root of the number of measurements. Since more
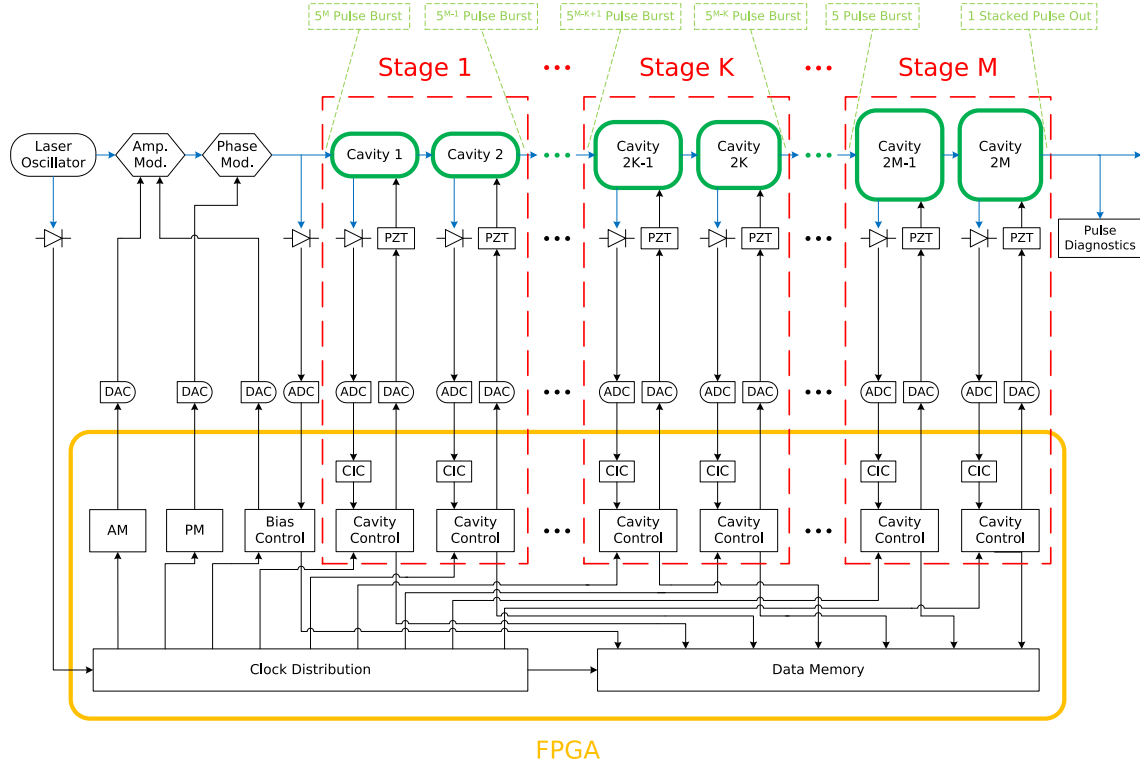
Fig. 11. FPGA-based large-scale feedback control system for coherent pulse stacking.

samples indicate noise reduction but higher latency, we have to trade off between the noise suppression and the loop delay.

All the above perturbations will ultimately translate into the pulse intensity fluctuations detected by the photodiode for each cavity. The pulse-pattern-based cavity phase detection algorithm gives a measurement error

$$\sigma_\varphi = \sqrt{\sum_{i=1}^{N}(a_i^2 + b_i^2)} \cdot \sigma_P, \tag{11}$$

where σ_φ is the cavity phase error and σ_P is the pulse intensity noise detected by the photodiode. After an optimized calibration, 1.0% level noise of the pulse intensity will lead to a 0.5 deg cavity phase error. Since noise performances of the algorithm are identical among different cavities, the measurement error induced by the algorithm will not scale with the multi-stage cavity phase stabilization. As the cavity size increases, the multi-stage CIC filter will be implemented for better noise suppression performance. With the most efficient cavity design, maintaining an 8.0 deg cavity phase error will reach 95% of the theoretical enhancement maximum and achieve a 20 dB satellite-pulse contrast ratio for each stage consisting of two cavities.

B. FPGA-Based Scaling Solution

The described novel model directly links the coherent pulse stacking physics to the digital control theory. Since it is convenient to extend the model to multi-stage cavity phase stabilization in the Z domain, this model is an essential tool for a scalable multiple-input and multiple-output (MIMO) scheme towards a distributed deterministic optical phase control.

The high-speed FPGA system has enough capacity to accommodate multi-stage coherent pulse stacking and large-scale feedback control, as shown in Fig. 11. Our scaling solution is to have intermediate monitoring points for each branch to increase the response bandwidth of the system, together with the state-of-the-art software-defined-radio digital signal processing in a distributed topology. It is easy to cascade one more cavity for stacking just by adding one distributed node consisting of a detector (one photodiode and one ADC) and an actuator (one slow DAC and one piezo) in hardware. With a fully modular firmware in the FPGA, multi-stage cavity phase stabilization can be done by repeatedly calling the "cavity control" module, so the FPGA complexity of the feedback control system is independent of the number M of the stacking stage. The FPGA containing gigabit transceivers provides a deterministic high-throughput data exchange network, which can overcome the limitation of communication latency between the master controller and distributed nodes. Leveraging of capabilities of high-speed data acquisition and parallel processing, the FPGA achieves a kHz-level control bandwidth for multi-cavity phase stabilization and paves a programmable way for scalability. For the large-scale deployment, since distributed nodes need to be synchronized to the master FPGA with a high precision, the femtosecond-level timing and synchronization technique can

also be included in the control system to guarantee the phase delay matching across distributed nodes [19], [20].

The bandwidth of the FPGA-based feedback control system is primarily limited by the resonant frequency of the piezo-driven mirror. In the large-scale coherent pulse stacking, upgrading the piezo-driven mirror will increase the whole system bandwidth, thus further improving the system performance in noise suppression. Another hurdle to FPGA-based system is that developing FPGA applications is a time-consuming process (due to difficult debugging and lengthy compilation time), which needs expertise both in firmware and hardware for exploiting the FPGA resources properly.

VI. Conclusion

In summary, based on the Z-transform model and the pulse-pattern-based cavity phase detection algorithm, the optical cavity phase control on FPGA with nm accuracy has been demonstrated over 12 hours, and ensures the multiplexed 2+1 cavities (15-pulse) stacking at a 1.2% level intensity stability. Since our control system is a distributed synchronous digitizer network with firmware and software integration for algorithms, this approach can be scaled to large numbers of cavities. Our near-term goal is to build a 3-stage (2+2+2 cavities) 125-pulse stacking system. This is of the scale that can enable fiber lasers to extract all available energy, while mitigating nonlinearity so that high energy, ultrafast pulses can be produced.

References

[1] E. Esarey, C. B. Schroeder, and W. P. Leemans, "Physics of laser-driven plasma-based electron accelerators," *Rev. Mod. Phys.*, vol. 81, no. 3, pp. 1229–1285, Aug. 2009.

[2] C. Danson, D. Hillier, N. Hopps, and D. Neely, "Petawatt class lasers worldwide," *High Power Laser Sci. Eng.*, vol. 3, p. e3, Jan. 2015.

[3] J. Dawson *et al.*, "Analysis of the scalability of diffraction-limited fiber lasers and amplifiers to high average power," *Opt. Exp.*, vol. 16, no. 17, pp. 13240–13266, Aug. 2008.

[4] T. Zhou, J. Ruppe, C. Zhu, I.-N. Hu, J. Nees, and A. Galvanauskas, "Coherent pulse stacking amplification using low-finesse Gires-Tournois interferometers," *Opt. Exp.*, vol. 23, no. 6, pp. 7442–7462, Mar. 2015.

[5] M. Kienel, M. Müller, A. Klenke, J. Limpert, and A. Tünnermann, "12 mJ kW-class ultrafast fiber laser system using multidimensional coherent pulse addition," *Opt. Lett.*, vol. 41, no. 14, pp. 3343–3346, Jul. 2016.

[6] L. Siiman, W.-Z. Chang, T. Zhou, and A. Galvanauskas, "Coherent femtosecond pulse combining of multiple parallel chirped pulse fiber amplifiers," *Opt. Exp.*, vol. 20, no. 16, pp. 18097–18116, Jul. 2012.

[7] M. Kienel, M. Müller, A. Klenke, T. Eidam, J. Limpert, and A. Tünnermann, "Multidimensional coherent pulse addition of ultrashort laser pulses," *Opt. Lett.*, vol. 40, no. 4, pp. 522–525, 2015.

[8] W.-Z. Chang, T. Zhou, L. A. Siiman, and A. Galvanauskas, "Femtosecond pulse spectral synthesis in coherently-spectrally combined multi-channel fiber chirped pulse amplifiers," *Opt. Exp.*, vol. 21, no. 3, pp. 3897–3910, Feb. 2013.

[9] T. M. Shay, "Theory of electronically phased coherent beam combination without a reference beam," *Opt. Exp.*, vol. 14, no. 25, pp. 12188–12195, Dec. 2006.

[10] M. Mueller, M. Kienel, A. Klenke, T. Eidam, J. Limpert, and A. Tünnermann, "Phase stabilization of spatiotemporally multiplexed ultrafast amplifiers," *Opt. Exp.*, vol. 24, no. 8, pp. 7893–7904, Apr. 2016.

[11] A. Galvanauskas *et al.*, "Coherent pulse stacking amplification - extending chirped pulse amplification by orders of magnitude," in *Proc. CLEO*, San Jose, CA, USA, May 2017, p. SM4I.1.

[12] F. Gires and P. Tournois, "Interferometre utilisable pour la compression dimpulsions lumineuses modulees en frequence," *Weekly Rep. Acad. Sci. Sessions*, vol. 258, pp. 6112–6115, Jun. 1964.

[13] T. Zhou, J. Ruppe, P. Stanfield, J. Nees, R. Wilcox, and A. Galvanauskas, "Resonant cavity based time-domain multiplexing techniques for coherently combined fiber laser systems," *Eur. Phys. J. Spec. Top.*, vol. 224, no. 13, pp. 2585–2602, Oct. 2015.

[14] D. Dahlen, R. Wilcox, and W. P. Leemans, "Modeling Herriott cells using the linear canonical transform," *Appl. Opt.*, vol. 56, no. 2, pp. 267–272, Jan. 2017.

[15] Y. Yang *et al.*, "A pulse-pattern-based phase-locking method for multi-cavity coherent pulse stacking," in *Proc. CLEO*, San Jose, CA, USA, May 2017, p. SM4I.3.

[16] R. Wilcox *et al.*, "Interferometer design and controls for pulse stacking in high power fiber lasers," in *Proc. AAC*, Oxon Hill, MD, USA, Aug. 2016.

[17] M. J. Martin and J. Ye, *Optical Coatings and Thermal Noise in Precision Measurement*. London, U.K.: Cambridge Univ. Press, 2012, ch. 15.

[18] E. Luzhansky, "Reaching stability horizons with isolated stable optical cavities," *Proc. SPIE*, Sep. 2012. [Online]. Available: http://spie.org/newsroom/4344-reaching-stability-horizons-with-isolated-stable-optical-cavities?SSO=1, doi: 10.1117/2.1201208.004344.

[19] R. Wilcox, J. M. Byrd, L. Doolittle, G. Huang, and J. W. Staples, "Stable transmission of radio frequency signals on fiber links using interferometric delay sensing," *Opt. Lett.*, vol. 34, no. 20, pp. 3050–3052, Oct. 2009.

[20] J. Kim, J. A. Cox, J. Chen, and F. X. Kärtner, "Drift-free femtosecond timing synchronization of remote optical and microwave sources," *Nature Photon.*, vol. 2, no. 12, pp. 733–736, Nov. 2008.

Yilun Xu received the B.S. degree from Tsinghua University, Beijing, China, in 2013, where he is currently pursuing the Ph.D. degree with the Department of Engineering Physics. He has been a Visiting Scholar with the Lawrence Berkeley National Laboratory since 2015. His research interests include control system for ultrafast laser, digital low level RF control system, femto-second timing and synchronization system for particle accelerators.

Russell Wilcox was born in San Jose, CA, USA, in 1957. He received the B.S.E.E. degree in electrical engineering from the University of California at Berkeley, Berkeley, in 1980. In 1980, he joined the Lawrence Livermore Laboratory, where he developed oscillators and pulse generating systems for fusion lasers, including the Nova and NIF facilities. Since 2003, he has been with the Lawrence Berkeley National Laboratory, where he developed cryogenically cooled TiSaf lasers, high precision timing systems for free electron lasers, and coherent addition methods for fiber lasers. He has received ten patents on laser and optical devices. His current research interests include high peak power fiber lasers and controls for coherent pulse addition.

John Byrd received the Degree in engineering physics from The University of Arizona in 1985, and the M.S. and Ph.D. degrees in accelerator physics from Cornell University in 1988 and 1991, respectively. He joined the Lawrence Berkeley National Laboratory in 1991, became the Group Leader in 2003, and has been the Program Head of the Center for Beam Physics since 2011. He joined the Argonne National Laboratory and became the Director of the Accelerator Systems Division in 2017. His research interests include high energy accelerators and next-generation synchrotron radiation sources. He is a fellow of the American Physical Society and a primary organizer for multiple topical workshops.

Lawrence Doolittle received the B.S. degree from the California Institute of Technology in 1979, and the Ph.D. degree in materials science from Cornell University in 1987. He joined the Jefferson Laboratory in 1987, and has been a Staff Engineer and Scientist with the Lawrence Berkeley National Laboratory since 1999. He is an expert on digital LLRF control, participating in the LLRF Projects with SLAC/LCLS/LCLS-II, Fermi@Elettra, Argonne/APS/SPX, and LBNL/APEX.

Qiang Du received the B.S. degree in engineering physics and the Ph.D. degree in nuclear engineering from Tsinghua University in 2001 and 2006, respectively. He has been an Assistant Professor with Tsinghua University since 2008. He joined the Lawrence Berkeley National Laboratory and became an Electronics Research Scientist and Engineer in 2013. He received the DOE Early Career Research Award for scalable control of multidimensional coherent pulse addition for high average power ultrafast lasers in 2017.
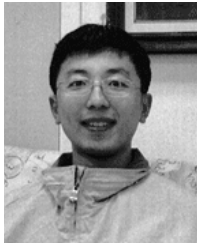
Gang Huang received the B.S. degree in engineering physics and the Ph.D. degree in accelerator technology and application from Tsinghua University in 1997 and 2002, respectively. He joined the Lawrence Berkeley National Laboratory in 2004. His research interests include low level RF control system for particle accelerators, femto-second timing and synchronization, and ultrafast beam diagnostic.

Yawei Yang received the B.S. and Ph.D. degrees from Tsinghua University, Beijing, China, in 2009 and 2014, respectively. He is currently a Physicist Post-Doctoral Fellow with the Lawrence Berkeley National Laboratory.
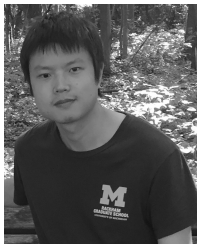
Tong Zhou received the B.S. and M.S. degrees from Peking University, Beijing, China, in 2007 and 2010, respectively, and the Ph.D. degree from the University of Michigan, Ann Arbor, USA, in 2015. He was a Research Fellow with the University of Michigan in 2015, and a Fiber Laser Engineer with Thorlabs, Inc. from 2015 to 2017. He is currently a Physicist Post-Doctoral Fellow with the Lawrence Berkeley National Laboratory.

Wim Leemans (S'88–M'90–SM'05–F'07) received the Degree in electrical engineering/applied physics from the Vrije Universiteit Brussel, Belgium, in 1985, and the M.S. and Ph.D. degrees in electrical engineering with emphasis on plasma physics from UCLA in 1987 and 1991, respectively. He joined the Lawrence Berkeley National Laboratory in 1991, became the Group Leader in 1993, and in 1995 started the LOASIS Program (Lasers, Optics and Accelerator Systems Integrated Studies). Since 2007, he has also been the Director of LOASIS, which is currently known as the BELLA (Berkeley Lab Laser Accelerator) Center. He has authored over 140 refereed papers; these papers have been cited well over 8000 times. His research interests include laser-based advanced accelerator concepts for electrons and radiation sources for supporting science and medical applications. His work has been recognized with several prestigious awards. He is a fellow of the APS and the AAAS. He has been a research advisor for over 15 Ph.D. graduate students, including two who received the APS Outstanding Dissertation Award in 2005 and 2006 and one who received the Japanese PJAS prize for Outstanding Dissertation in 2007.

Almantas Galvanauskas was born in Vilnius, Lithuania, in 1963. He received the Diploma degree in physics from Vilnius University, Vilnius, Lithuania, in 1986, and the Ph.D. degree in physics from the Royal Institute of Technology, Stockholm, Sweden, in 1992. From 1993 to 2001, he was with IMRA America Inc., Ann Arbor, MI, where he was involved in research and development of high-energy and high-power femtosecond fiber laser technology. He joined the University of Michigan in 2002. He is currently a Professor with the Electrical Engineering and Computer Science Department, University of Michigan. He has been involved with fiber lasers for approximately 20 years, and has over 200 publications, including approximately 30 patents and patent applications. He had pioneered ultrashort-pulse fiber CPA and his work had resulted in demonstrating several record-breaking achievements in the performance of fiber lasers. His current work spans areas from novel fiber designs to advanced fiber laser systems, including beam combining of pulsed and ultrashort pulse lasers, and new fiber laser applications such as high-intensity laser plasma produced EUV and X-ray generation. He is also a Co-Founder of Arbor Photonics, Inc. He is a member of the Optical Society of America.

John Ruppe received the B.S. degree from Cornell University in 2012. He is currently pursuing the Ph.D. degree with the Center for Ultrafast Optical Science, University of Michigan. He is currently on a team to design an ultrafast fiber laser system.

Chuanxiang Tang received the B.S. degree in modern physics and applications and the M.S. and Ph.D. degrees in accelerator physics and applications from Tsinghua University in 1992 and 1996, respectively. He was a Guest Scientist with DESY from 1996 to 1998. He has been a Professor with Tsinghua University since 2004. He was the Director of the Department of Engineering Physics from 2006 to 2012. His research interests include accelerator physics and beam dynamics. He is a member of the administrative council and the Group Leader of the Accelerator Physics Specialized Group with the China Particle Accelerators Society. He received the New Century Excellent Talents in University Award in 2004 and the China National Funds for Distinguished Young Scientists in 2009.

Wenhui Huang received the B.S. degree in applied physics and the Ph.D. degree in accelerator physics from Tsinghua University in 1999. He was a Guest Scientist with DESY from 2000 to 2001. He is currently a Professor and the Deputy Director of the Department of Engineering Physics, Tsinghua University. His research interests include beam-instability of high energy circular accelerator.